



Entanglement generation and steering implementation in a double-cavity-magnon hybrid system

LONG-JIANG CONG,¹ YI-XIONG LUO,¹ ZHI-GANG ZHENG,¹
HONG-YU LIU,^{1,5}  YING MING,^{1,6}  AND RONG-CAN YANG^{2,3,4,7}

¹College of Science, Yanbian University, Yanji, Jilin 133002, China

²College of Physics and Energy, Fujian Normal University, Fujian Provincial Key Laboratory of Quantum Manipulation and New Energy Materials, Fuzhou, 350117, China

³Fujian Provincial Engineering Technology Research Center of Solar Energy Conversion and Energy Storage, Fuzhou, 350117, China

⁴Fujian Provincial Collaborative Innovation Center for Advanced High-Field Superconducting Materials and Engineering, Fuzhou, 350117, China

⁵liuhongyu@ybu.edu.cn

⁶mingying@ybu.edu.cn

⁷rcyang@fjnu.edu.cn

Abstract: We demonstrate a scheme for the generation of bipartite and tripartite entanglement, as well as the implementation of stable and controllable long-distance one-way and asymmetric two-way steering in a cavity-magnon hybrid system. This system consists of a magnon mode and two coupled microwave cavities. The first cavity is driven by a flux-driven Josephson parametric amplifier, which generates squeezed vacuum fields, and is coupled to the other cavity through optical tunneling interaction. The second cavity and magnon mode are coupled through magnetic dipole interaction. We find that under weak coupling between the two cavities, and strong coupling between the second cavity and magnon mode, remote controllable one-way steering and tripartite entanglement can be achieved. Our scheme may have potential applications in quantum information.

© 2023 Optica Publishing Group under the terms of the [Optica Open Access Publishing Agreement](#)

1. Introduction

In 1935, Einstein, Podolsky, and Rosen (EPR) made a famous argument—whether quantum mechanics is complete. To make an end of the argument, Schrödinger introduced the term "entanglement" [1–3]. With consideration of complexity, many researchers mainly focus on bipartite and tripartite entanglement. It is known that bipartite ones refer to the states shared by two parties which cannot be described separately, while tripartite ones refer to the states shared by three or more parties can also not be described individually but only through the collective state [4–7]. Up to now, quantum entanglement is proved to be significant because it offers a new way to describe the connection and interaction between bi/multi-body quantum systems [8,9]. Different from entanglement, quantum steering is the process of acquiring information about an unmeasurable quantum system by measuring a single quantum system [10,11]. These concepts have numerous applications in the field of quantum science and technology, including Bell inequality testing [12,13], quantum information processing [14], quantum precision measurement [15], quantum key distribution [16,17], and quantum teleportation [18,19]. However, despite extensive research and experimental demonstration of quantum entanglement and quantum steering between continuous-variable states or between discrete-variable ones are proposed [20–27], achieving unidirectional quantum steering with flexibility and controllability remains challenging. Consequently, researchers are investigating directional quantum steering, with a particular focus on unidirectional quantum steering, to enhance its capabilities.

For the realization of quantum entanglement and quantum steering, we know that mixed quantum systems such as cavity optomechanical systems and cavity-magnetic hybrid systems attract a lot of attention [28–33]. Among them, the cavity magnetic hybrid system is particularly attractive [34–36]. The reason is that the Kittel mode, a spatially uniform mode of spin waves within magnetic materials can be strongly coupled to microwave photons [36–41]. Among these structures, the cavity-magnon hybrid system, which mainly studies the interaction between microwave photons and ferromagnetic materials such as Yttrium Iron Garnet (YIG) crystals, has become a focus. Because YIG crystals that are easy to magnetize [42,43] have low dissipation rates and are therefore more desirable for various ferromagnetic materials. Additionally, both optical and microwave cavities can confine photons to enhance the coupling rate between photons and matter, providing a wider range of experimental applications for quantum information science [39,44,45]. Furthermore, Josephson Parametric Amplifier (JPA) driven by flux can be used for signal compression, effectively reducing the signal bandwidth, and improving the signal transmission efficiency [46,47]. The compression principle of the JPA is based on the principle of quantum measurement, which converts the frequency information of the signal into amplitude information by interfering the signal with a reference signal, achieving signal compression.

In this study, we demonstrate the bipartite and tripartite entanglement and directional remote controllable steering of the cavity-magnon hybrid system. To enhance operational flexibility, we utilized two separate cavities. The controllability of the system is achieved by modifying various parameters, such as adjusting the distance between the microwave cavities to alter the cavity-cavity coupling rate J , and changing the coupling strength g_{ma} by manipulating the bias magnetic field direction and the position of the YIG sphere [43]. Our research illustrates that a remote tripartite entanglement can be generated and a remote controllable unidirectional steering can be realized. They are steady and robust, leading them to have many potential applications for remote quantum information science.

This paper is organized as follows: In Sec. II, we present our model and the corresponding Hamiltonian, and then analyze quantum correlations in Sec. III; numerical simulations are conducted in the fourth section; and, finally, the conclusion of this paper is presented in the fifth section.

2. Model and Hamiltonian

We consider a hybrid system consisting of two microwave cavities and a YIG sphere, as depicted in Fig. 1. Cavity 1 (marked as a_1) is driven by a weak squeezed vacuum field using a JPA with a flux, while cavity 2 (marked as a_2) is directly coupled to the Kittel mode confined in YIG sphere which is trapped in the cavity 2 through a magnetic dipole interaction, and the two microwave cavities interact with each other through a microwave wire. It is assumed that YIG sphere's size is much smaller than the microwave wavelength, rendering the effect of radiation pressure negligible [48–50]. Thus, the Hamiltonian of the entire system can be presented below by

$$H/\hbar = \sum_{j=1}^2 \omega_j a_j^\dagger a_j + \omega_m m^\dagger m + J(a_1^\dagger a_2 + a_1 a_2^\dagger) + g_{ma}(a_2^\dagger m + a_2 m^\dagger) \quad (1)$$

where a_j^\dagger , m^\dagger (a_j , m) are the creation (annihilation) operators of the j th cavity mode and magnon mode, respectively, satisfying the standard bosonic commutation relations. Without loss of generalization, frequencies of the j th cavity mode and magnon mode are denoted by ω_j and ω_m , respectively. It is known that ω_m can be significantly altered by varying the strength of the bias magnetic field in the z direction, and their mathematical relationship is $\omega_m = \gamma H$ with H the strength of the bias magnetic field and γ representing the gyromagnetic ratio of YIG material

and its value being $\gamma/2\pi = 28$ GHz/T. In addition, J denotes the interaction rate between the two cavities, which can be adjusted by changing the wire length, while g_{ma} is the coupling strength between cavity 2 and the magnon, which can be tuned by varying the direction of the bias magnetic field and the position of the YIG sphere [43]. Moreover, the weak squeezed vacuum field has a frequency ω_s when a pump frequency of $2\omega_s$ acting on JPA [46,51–60]. In the rotating frame with the frequency ω_s , the rotating Hamiltonian for the system is

$$H_{\text{eff}}/\hbar = \sum_{j=1}^2 \Delta_j a_j^\dagger a_j + \Delta_m m^\dagger m + J \left(a_1^\dagger a_2 + a_1 a_2^\dagger \right) + g_{ma} \left(a_2^\dagger m + a_2 m^\dagger \right) \quad (2)$$

with $\Delta_j = \omega_j - \omega_s$, $\Delta_m = \omega_m - \omega_s$. In this case, the corresponding quantized Langevin equations can be obtained and described by

$$\begin{aligned} \dot{a}_1 &= -i\Delta_1 a_1 - iJ a_2 - \kappa_1 a_1 + \sqrt{2\kappa_1} a_1^{\text{in}}, \\ \dot{a}_2 &= -i\Delta_2 a_2 - iJ a_1 - i g_{ma} m - \kappa_2 a_2 + \sqrt{2\kappa_2} a_2^{\text{in}}, \\ \dot{m} &= -i\Delta_m m - i g_{ma} a_2 - \kappa_m m + \sqrt{2\kappa_m} m^{\text{in}}, \end{aligned} \quad (3)$$

where κ_1 , κ_2 , and κ_m (a_1^{in} , a_2^{in} and m^{in}) are the dissipation rates (input noise operators) of the j th cavity and magnon mode, respectively. In this scheme, JPA is utilized to manipulate the noise characteristics of the quantum fluctuations in the cavity field, leading to a squeezed cavity field. As a result, the input noise operators have a zero mean and are defined by the subsequent correlation functions [61]: $\langle a_1^{\text{in}\dagger}(t) a_1^{\text{in}}(t') \rangle = N\delta(t-t')$, $\langle a_1^{\text{in}}(t) a_1^{\text{in}\dagger}(t') \rangle = (N+1)\delta(t-t')$, $\langle a_1^{\text{in}}(t) a_1^{\text{in}}(t') \rangle = M\delta(t-t')$

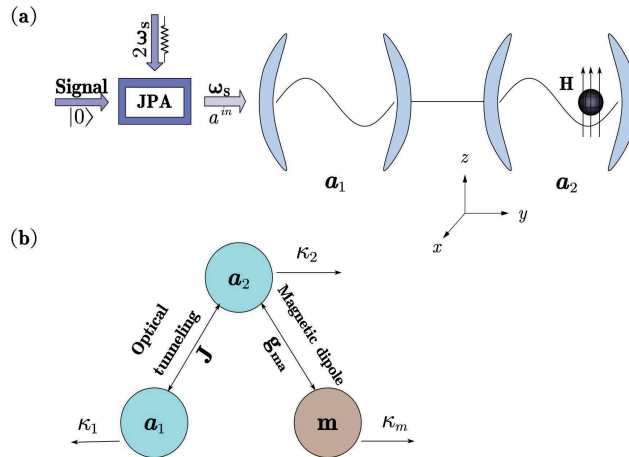


Fig. 1. Sketch of cavity-magnon hybrid system. (a) The YIG sphere is positioned within cavity 2 on the right, while the microwave field in cavity 1 on the left is stimulated by a weak squeezed vacuum field generated by a Josephson parametric amplifier, which is driven by a flux. The bias magnetic field that produces the Kittel mode is along the z-axis, whereas the magnetic field that generates the cavity mode is along the $\pm y$ -axis. (b) The figure below depicts the coupling between the magnon mode and two cavity modes. The two cavities are directly coupled through optical tunneling with a coupling strength of J . The cavity 2 and magnon are directly coupled through magnetic dipole interaction with a coupling strength of g_{ma} . The j th cavity mode and magnon mode have dissipation rates κ_1 , κ_2 , and κ_m , respectively.

t'), $\langle a_1^{in\dagger}(t)a_1^{in\dagger}(t') \rangle = M^* \delta(t-t')$, $\langle a_2^{in\dagger}(t)a_2^{in\dagger}(t') \rangle = n_2 \delta(t-t')$, $\langle a_2^{in}(t)a_2^{in\dagger}(t') \rangle = (n_2 + 1) \delta(t-t')$, $\langle m^{in\dagger}(t)m^{in\dagger}(t') \rangle = n_m \delta(t-t')$, $\langle m^{in}(t)m^{in\dagger}(t') \rangle = (n_m + 1) \delta(t-t')$, $N = (n_1 + 1) \sinh^2 r + n_1 \cosh^2 r$, $M = (2n_1 + 1)e^{i\theta} \sinh r \cosh r$, and $n_o = 1/[\exp(\frac{\hbar\omega_o}{k_B T}) - 1]$ ($o = 1, 2, m$), where r is the squeezing parameter and θ is the phase of the squeezed field.

3. Entanglement and steering

To quantify the system, three sets of orthogonal components are introduced, i.e. $X_1^{in} = (a_1^{in\dagger} + a_1^{in})/\sqrt{2}$, $Y_1^{in} = i(a_1^{in\dagger} - a_1^{in})/\sqrt{2}$, $X_2^{in} = (a_2^{in\dagger} + a_2^{in})/\sqrt{2}$, $Y_2^{in} = i(a_2^{in\dagger} - a_2^{in})/\sqrt{2}$, $X_m^{in} = (m^{in\dagger} + m^{in})/\sqrt{2}$, $Y_m^{in} = i(m^{in\dagger} - m^{in})/\sqrt{2}$. In this case, the linear quantum Langevin equations can be rewritten in a matrix form expressed by

$$\dot{\sigma}(t) = A\sigma(t) + \mu(t), \quad (4)$$

where $\sigma(t) = [X_1^{in}(t), Y_1^{in}(t), X_2^{in}(t), Y_2^{in}(t), X_m^{in}(t), Y_m^{in}(t)]^T$, $\mu(t) = [\sqrt{2\kappa_1}X_1^{in}(t), \sqrt{2\kappa_1}Y_1^{in}(t), \sqrt{2\kappa_2}X_2^{in}(t), \sqrt{2\kappa_2}Y_2^{in}(t), \sqrt{2\kappa_m}X_m^{in}(t), \sqrt{2\kappa_m}Y_m^{in}(t)]^T$ are vectors of quantum fluctuations and quantum noise, respectively and

$$A = \begin{bmatrix} -\kappa_1 & \Delta_1 & 0 & J & 0 & 0 \\ -\Delta_1 & -\kappa_1 & -J & 0 & 0 & 0 \\ 0 & J & -\kappa_2 & \Delta_2 & 0 & g_{ma} \\ -J & 0 & \Delta_2 & -\kappa_2 & -g_{ma} & 0 \\ 0 & 0 & 0 & g_{ma} & -\kappa_m & \Delta_m \\ 0 & 0 & -g_{ma} & 0 & -\Delta_m & -\kappa_m \end{bmatrix}, \quad (5)$$

is the drift matrix of the system.

Due to the linearity of the Langevin equation and the Gaussian nature of quantum noise, the system will decay to a stationary Gaussian state, which can be fully characterized by the 6×6 covariance matrix (CM) \mathcal{V} in phase space: $\mathcal{V}_{ij} = [\langle \sigma_i(t)\sigma_j(t') + \sigma_j(t')\sigma_i(t) \rangle]/2$, ($i, j = 1, 2, \dots, 6$). In this manuscript, we focus on the stationary CM \mathcal{V} which can be directly obtained by solving the Lyapunov equation [62],

$$A\mathcal{V} + \mathcal{V}A^T = -D, \quad (6)$$

with

$$D = \begin{bmatrix} \kappa_{a_1} & \kappa_{a_2} & 0 & 0 & 0 & 0 \\ \kappa_{a_2} & \kappa_{a_3} & 0 & 0 & 0 & 0 \\ 0 & 0 & \kappa_{a_4} & 0 & 0 & 0 \\ 0 & 0 & 0 & \kappa_{a_4} & 0 & 0 \\ 0 & 0 & 0 & 0 & \kappa_{a_5} & 0 \\ 0 & 0 & 0 & 0 & 0 & \kappa_{a_5} \end{bmatrix}, \quad (7)$$

where $\kappa_{a_1} = \kappa_1(2N + 1 + M + M^*)$, $\kappa_{a_2} = i\kappa_1(M^* - M)$, $\kappa_{a_3} = \kappa_1(2N + 1 - M - M^*)$, $\kappa_{a_4} = (2n_2 + 1)\kappa_2$, $\kappa_{a_5} = (2n_m + 1)\kappa_m$.

It is known that the Lyapunov equation can be solved to obtain \mathcal{V} , and then to quantify quantum entanglement for the system or subsystems. For this end, it is convenient to use logarithmic negativity (LN) EN_{ij} and minimum residual entanglement (MRE) R_{τ}^{\min} to separately quantify

bipartite and tripartite entanglement for the subsystem (denoted as $i, j = 1, 2, m$ and $i \neq j$) and the whole system [63–65], whose mathematical equations are defined as [48,66,67]

$$EN_{ij} = \max[0, -\ln(2v_{ij})] \quad (8)$$

and

$$R_{\tau}^{\min} = \min[R_{\tau}^{1|2m}, R_{\tau}^{2|1m}, R_{\tau}^{m|12}], \quad (9)$$

where $R_{\tau}^{i|jk} \equiv C_{i|jk} - C_{i|j} - C_{i|k} \geq 0$ ($i \neq j \neq k, i \neq k$), $C_{i|j} = EN_{ij}^2$ is the contangle of subsystems i and j with $v_{ij} = \sqrt{E_{ij} - (E_{ij}^2 - 4R_{ij}^2)^{1/2}}$, $E_{ij} = R_1^{ij} + R_2^{ij} - 2R_3^{ij}$, $R_1^{ij} = \det V_1^{ij}$, $R_2^{ij} = \det V_2^{ij}$, $R_3^{ij} = \det V_3^{ij}$, $R_{ij} = \det V_m^{ij}$, with

$$V_m^{ij} = \begin{bmatrix} V_1^{ij} & V_3^{ij} \\ V_3^{ijT} & V_2^{ij} \end{bmatrix}, \quad (10)$$

$V_1^{ij}, V_2^{ij}, V_3^{ij}$ are submatrices of V_m^{ij} with the dimension 2×2 , and $C_{i|jk} = EN_{i|jk}^2$, $EN_{i|jk} = \max[0, -\ln 2v_{i|jk}]$ with $v_{i|jk} = \min \text{eig} | [\oplus_{s=1}^3 (-\sigma_y)] \mathcal{P}_{i|jk} \mathcal{V} \mathcal{P}_{i|jk} |$ in which $\mathcal{P}_{1|2m} = \sigma_z \oplus I \oplus I$, $\mathcal{P}_{2|1m} = I \oplus \sigma_z \oplus I$ and $\mathcal{P}_{m|12} = I \oplus I \oplus \sigma_z$ are the matrices for partial transposition at the level of CMs [66]. A nonzero minimum residual contangle $R_{\tau}^{\min} > 0$ indicates the presence of genuine tripartite entanglement in the system. $R_{\tau}^{i|jk} > 0$ is analogous to the Coffman-Kundu-Wootters monogamy inequality for three qubits [68].

Similarly, quantum steering for a bipartite subsystem is given as follows by [69]

$$\begin{aligned} G_{i \rightarrow j} &= \max \left[0, \frac{1}{2} \ln \frac{R_1^{ij}}{4R_2^{ij}} \right], \\ G_{j \rightarrow i} &= \max \left[0, \frac{1}{2} \ln \frac{R_2^{ij}}{4R_1^{ij}} \right], \\ G &= |G_{i \rightarrow j} - G_{j \rightarrow i}|. \end{aligned} \quad (11)$$

Here, $G_{i \rightarrow j}$ ($i \neq j$) represents the steering direction from i to j , and G denotes the differences for these two cases.

4. Numerical results and analysis

In the study of the cavity-magnon hybrid system, it is necessary to select optimal detunings to ensure the realization of entanglement and steering. At a low temperature of $T = 20$ mK, we set frequency detunings with respect to the squeezed light for cavity 1 and cavity 2 to be equal for convenience, i.e. $\Delta_1 = \Delta_2 = \Delta$. The YIG sphere used in the study has a diameter of 250 microns, a spin density of $\rho \approx 4.22 \times 10^{27} \text{ m}^{-3}$, and a total number of spins given by $N_{YIG} = V\rho \approx 3.45 \times 10^{16}$, where V is the volume of the sphere. Additionally, we choose experimentally accessible parameters [42,43]: $\omega_1/2\pi = \omega_2/2\pi = 10$ GHz, $\omega_m/2\pi = 10$ GHz, $\kappa_1/2\pi = \kappa_2/2\pi = 5$ MHz, $\kappa_m/2\pi = 1$ MHz. To obtain optimal detuning, we draw a graph illustrating the entanglement between the distant entangled cavity 1 and the magnon mode, as depicted in Fig. 2. Our findings indicate that the highest level of entanglement is achieved at $\Delta \approx 0$ and $\Delta_m \approx 0$. Therefore, in the following passages, we only take $\Delta = 0$ and $\Delta_m = 0$ into account for the sake of simplicity.

In addition to the frequency detunings, let us further confirm optimal values of the cavity-magnon coupling rate g_{ma} and cavity-cavity coupling rate J , we draw Fig. 3 which illustrates that distant and controllable one-way steering can be achieved when the ratio of the magnon-cavity coupling rate to the cavity-cavity coupling rate increases (supposed that the cavity-cavity coupling rate J and the input of JPA are fixed). We can achieve distant and controllable one-way steering, the applicable range is relatively large ($g_{ma}/J \in [4.8249, 4.47]$). As the ratio continues to increase

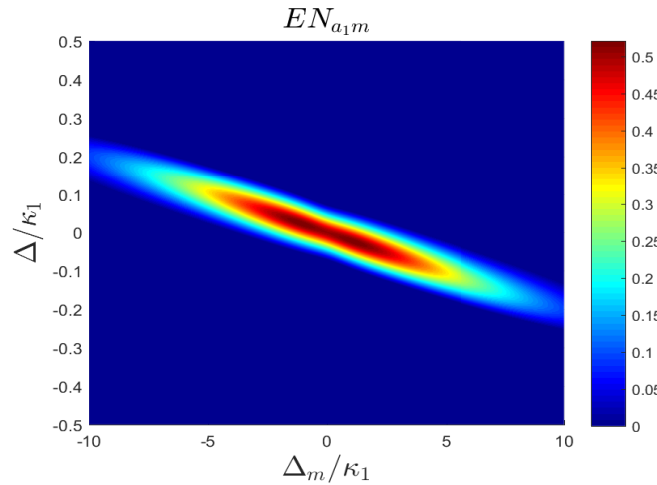


Fig. 2. Sketch of the indirect entanglement between cavity 1 and the magnon, with corresponding detunings Δ_m and Δ . Here, we set $J = \kappa_1$, $g_{ma} = 7\kappa_1$, $r = 2$, $\theta = 0$.

beyond $g_{ma}/J > 9.447$, distant and controllable asymmetric two-way steering can also be achieved. This finding has significant implications in unidirectional secure and device-independent quantum key distribution, where only one party's measurement apparatus is untrusted. Consequently, this process plays a vital role in quantum information.

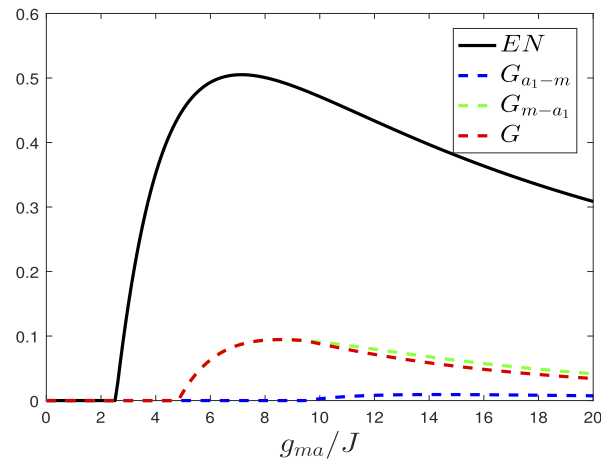


Fig. 3. Sketch of the indirect entanglement between cavity 1 and the magnon (solid black line), as well as the one-way steering from cavity 1 to the magnon (blue dashed line), the one-way steering from the magnon to cavity 1 (green dashed line), and the asymmetric steering (red dashed line). We choose $\Delta = \Delta_m = 0$, $J = \kappa_1$, $r = 2$, $\theta = 0$, $T = 20$ mK.

Next, let us consider the effect of squeezed parameter r and cavity-magnon (cavity) coupling rate $g_{ma}(J)$ on bipartite entanglement, we draw Fig. 4, where we have set (a) $J = \kappa_1$, $r = 0.66$; (b) $J = \kappa_1$, $r = 2$; (c) $g_{ma} = 7\kappa_1$, $r = 0.66$; (d) $g_{ma} = 7\kappa_1$, $r = 2$, and the other parameters $\Delta = 0\kappa_1$, $\Delta_m = 0.65\kappa_1$, $T = 20$ mK, $\theta = 0$. Our objective is to achieve the entanglement between cavity 1 and the magnon mode, so as to gain more precise control and utilization of this remote entanglement, thereby achieving more efficient quantum computation and more secure quantum communication. From Fig. 4 (a), we can see that when the cavity-magnon coupling coefficient

is 0, only entanglement between cavity 1 and cavity 2 appears. This is because we have fixed the cavity-cavity coupling to be non-zero, so in the case where cavity 2 is decoupled from the magnon, entanglement between cavity 1 and cavity 2 appears. As the cavity-magnon coupling coefficient increases, entanglement between cavity 2 and the magnon appears, and we find that entanglement between cavity 1 and cavity 2 also increases. This indicates that the magnon has a gain on cavity 2, and this gain will be transferred to cavity 1 as the cavity-magnon coupling coefficient continues to increase, leading to entanglement between cavity 1 and the magnon. In Fig. 4 (b), only entanglement between cavity 1 and the magnon appears when $r = 2$, and the maximum entanglement value is much larger than that at $r = 0.66$. In Fig. 4 (c), we have chosen a cavity-magnon coupling rate in the strong coupling region, so the dominant entanglement is between cavity 1 and the magnon. Similarly, as the cavity-cavity coupling coefficient increases, the dominant entanglement is the entanglement between cavity 1 and the magnon. Figure 4 (d) shows that when cavity 1 and cavity 2 are far apart (with a small cavity-cavity coupling coefficient), we can obtain the desired entanglement. As the cavity-cavity and cavity-magnon coupling rates continue to increase, the entanglement will eventually disappear. This is because within a certain range, the strength of the coupling is positively correlated with the entanglement, but when the coupling strength is too large, the quantum system will undergo degradation, leading to a decrease in entanglement.

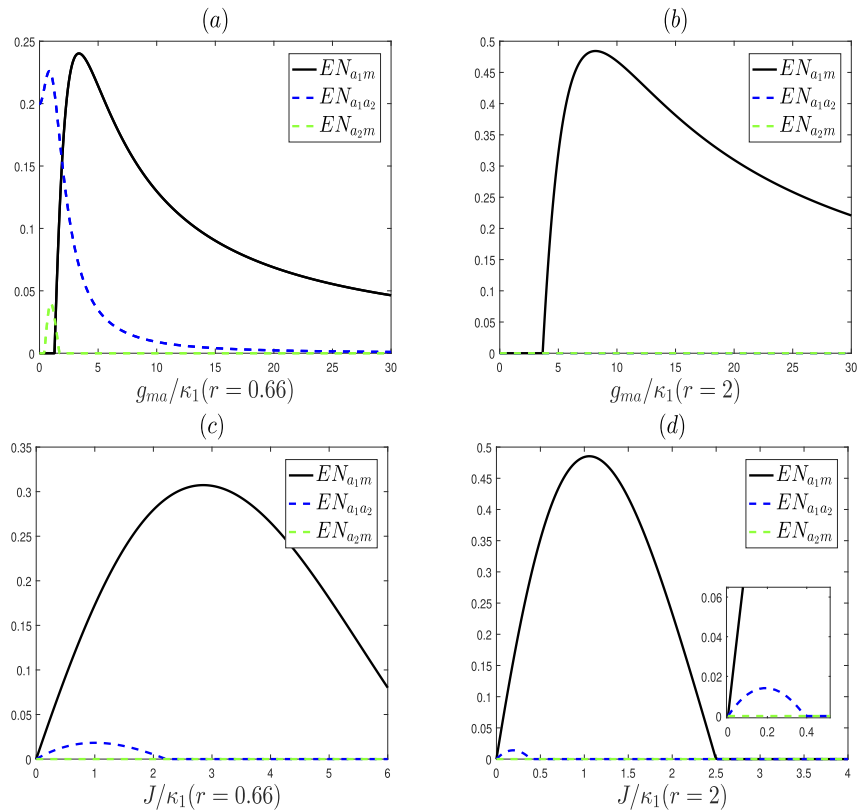


Fig. 4. Bipartite entanglement as a function of cavity-magnon coupling rate g_{ma} and cavity-cavity coupling coefficient J , (a) $J = \kappa_1$, $r = 0.66$; (b) $J = \kappa_1$, $r = 2$; (c) $g_{ma} = 7\kappa_1$, $r = 0.66$; (d) $g_{ma} = 7\kappa_1$, $r = 2$, and the other parameters are chosen as $\Delta = 0\kappa_1$, $\Delta_m = 0.65\kappa_1$, $T = 20\text{mK}$, $\theta = 0$.

Now, let us turn to study controllable one-way quantum steering. We demonstrate the steering as a function of coupling coefficients, which is depicted in Fig. 5. Within our selected parameter range, we observe only remote steering, which is one-way steering between cavity 1 and the magnon. In Fig. 5 (a), if we choose weak coupling rate J between the cavities, then one-way and asymmetric bidirectional steering occur at a greater distance as the cavity-magnon coupling coefficient increases. With increasing cavity-cavity coupling strength in Fig. 5 (b), asymmetric bidirectional steering and one-way steering from the magnon to cavity 1 appears, and we find that the best coupling coefficient is in the weak coupling region between the cavities, indicating the achievement of distant one-way steering. This demonstrates that the primary factor in our system is the distant steering between the magnon and cavity 1. We also found that unidirectional steering occurs even at very low (long distance) cavity 1 - cavity 2 coupling rates, which aligns with our objective. This design simplifies system structure and management, reduces complexity and unnecessary repetition, and enhances system stability and efficiency in practical applications.

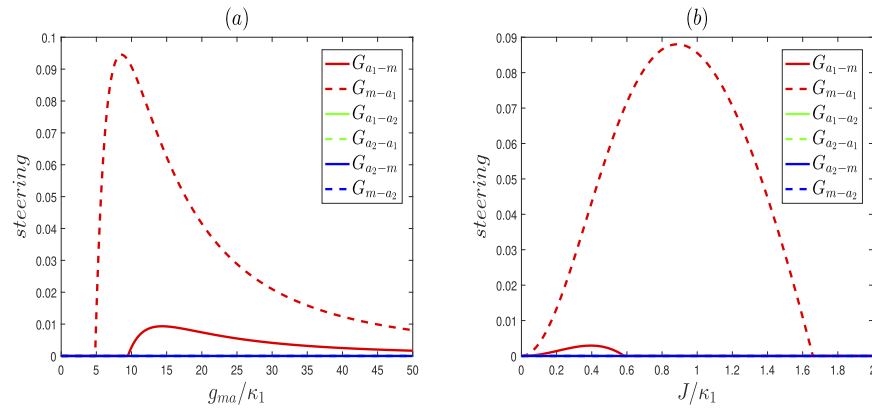


Fig. 5. Sketch of steering lines: steering from cavity 1 to the magnon (solid red line), steering from the magnon to cavity 1 (dashed red line), steering from cavity 1 to cavity 2 (solid green line), steering from cavity 2 to cavity 1 (dashed green line), steering from cavity 2 to the magnon (solid blue line), and steering from the magnon to cavity 2 (dashed blue line). We choose (a) $J = \kappa_1$, (b) $g_{ma} = 7\kappa_1$. Other parameters are $\Delta = \Delta_m = 0$, $r = 2$, $\theta = 0$, and $T = 20$ mK.

It should be noted that in Fig. 4, we have already observed the impact of the squeezing coefficient r on entanglement. In order to demonstrate the effect of the squeezing coefficient r on entanglement and steering more comprehensively, we depict Fig. 6, where the entanglement and steering of the distant steering cavity 1 and magnon particles were plotted, as shown in Fig. 6. The plot in Fig. 6 (a) illustrates that as the squeezing parameter r increased, the entanglement first increased and then decreased. Moreover, when $1.173 < r < 2.829$, indirect (distant) entanglement was the only type present, indicating that the squeezing parameter r can be controlled to obtain the desired indirect (distant) entanglement. The graph in Fig. 6 (b) shows that as the squeezing parameter r increased, an increase in the distant magnon to cavity 1 asymmetric bidirectional steering and unidirectional steering were observed. The maximum steering position was observed at $r = 2$, this is easily available experimentally. It is noted that the only resource for the entanglement and steering is cavity photons squeezed from JPA. According to Ref. [70], interference can occur between two two-photon quantum source. Thus, the squeezed phase θ for JPA can scarcely affect the entanglement and steering in our proposal.

We should note that many previous scheme for the preparation of entanglement is sensitive to environmental temperature, limiting the application of entanglement for quantum communications. Thus, in order to verify how robust our scheme is against environmental temperature, we depict

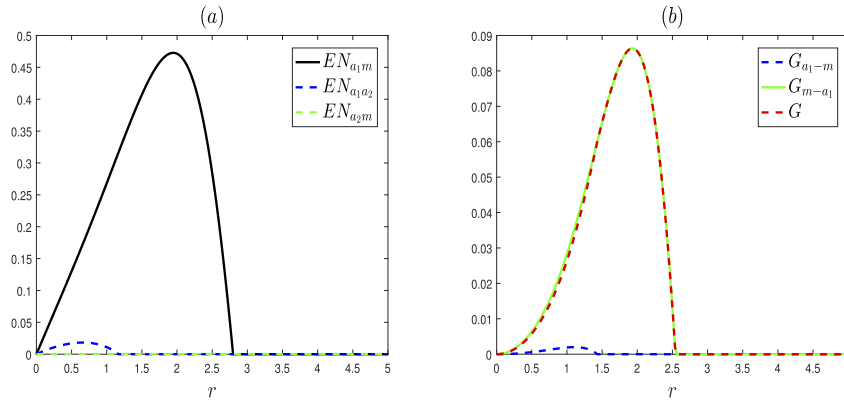


Fig. 6. Bipartite entanglement and the distant steering as a function of squeezing parameter r . (a) $\Delta = 0\kappa_1$, $\Delta_m = 0.65\kappa_1$, $T = 20$ mK, $\theta = 0$, $g_{ma} = 7\kappa_1$, $J = \kappa_1$. (b) $\Delta = \Delta_m = 0$, $\theta = 0$, $T = 20$ mK, $g_{ma} = 7\kappa_1$, $J = \kappa_1$.

Fig. 7, where we have illustrated the entanglement between the distant entanglement cavity 1 and magnon, along with the corresponding time graph for controllable unidirectional steering of the distant magnon to cavity 1. Our findings indicate that the practical range of entanglement for our system is $T \in [0, 0.344]$ K, whereas the practical range of the distant steering corresponds to $T \in [0, 0.152]$ K. It is noteworthy that steering is more sensitive to environmental temperature than entanglement. Nonetheless, our model can be realized within the experimental parameter range.

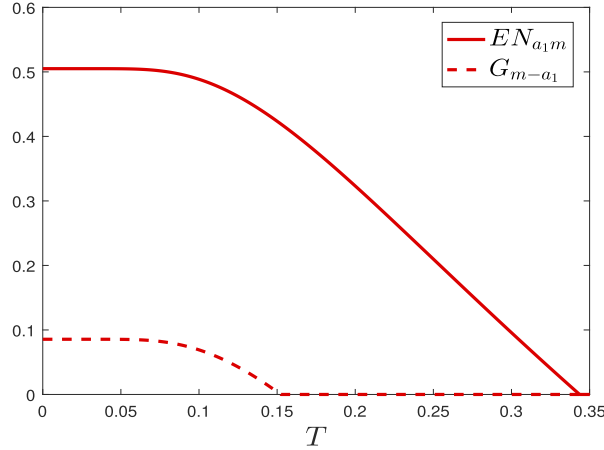


Fig. 7. Sketch of the entanglement between the distant entanglement cavity 1 and magnon, as well the graph of the corresponding temperature for unidirectional steering of the distant magnon to cavity 1. We selected $\Delta = \Delta_m = 0$, $\theta = 0$, $g_{ma} = 7\kappa_1$, $J = \kappa_1$, $r = 2$.

Finally, let us consider the entanglement for the whole system, i.e. tripartite entanglement. Figure 8 displays the graph of tripartite entanglement as a function of the squeezing parameter r in Fig. 8 (a) and detuning in Fig. 8 (b). The graph in Fig. 8 (a) demonstrates that our system exhibits tripartite entanglement, with the peak position occurring at $r = 1.239$. Substituting $r = 1.239$ into the graph of Fig. 8 (b), we observed that the maximum entanglement position is in proximity to the resonance position between the cavity and magnon. This result is consistent with the initial bipartite entanglement and verifies the validity of our approach. The presence of tripartite

entanglement in our system suggests its potential application in quantum key distribution, which exploits the unique properties of quantum entanglement for secure communication. In other word, by leveraging tripartite entanglement, parties involved in communication can establish a highly secure key to ensure the confidentiality of information transmission [71].

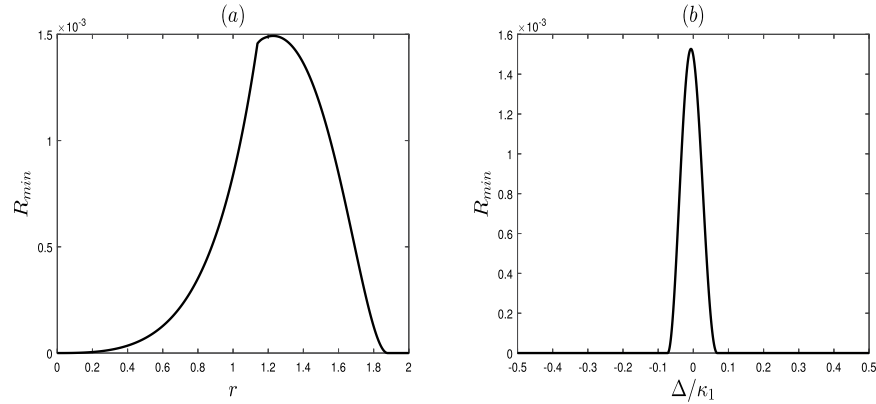


Fig. 8. Graph of the entanglement of the tripartite entanglement corresponding to squeezing parameter r and detuning. We selected $\Delta = 0\kappa_1$, $\Delta_m = 0.65\kappa_1$, $T = 20$ mK, $\theta = 0$, $g_{ma} = 7\kappa_1$, $J = 1\kappa_1$.

The parameters we have selected are within the feasible range of experimental parameters [42,43]. Our system is flexible and controllable, allowing us to adjust the distance between the two cavities to vary the strength of the coupling J . We can also achieve the desired entanglement and steering under weak coupling between the cavities. The coupling strength g_{ma} between cavity 2 and the magnon can be adjusted by changing the direction of the bias magnetic field and the position of the YIG sphere [43]. The compression introduced by the JPA is also within the scope of our experimental capabilities.

5. Conclusion

In summary, the presented cavity-magnon system consisting of two microwave cavities and a magnon mode can achieve tripartite entanglement, as well as distant controllable one-way and asymmetric two-way steering. Our scheme introduces noise to the subsystem through JPA, which enables the manipulation of unidirectional and asymmetric quantum steering through JPA or coupling parameters. The entanglement and steering exhibit high stability with respect to temperature. Thus, the cavity-magnon system can achieve tripartite entanglement, one-way steering, and asymmetric two-way steering. Our system has significant potential for application in the field of quantum information.

Funding. Natural Science Foundation of Fujian Province (2021J01185); National Natural Science Foundation of China (12174055, 62165014).

Acknowledgements. This work is supported by National Natural Science Foundation of China (Grant No. 62165014 and 12174055) and Fujian Natural Science Foundation (Grant No. 2021J01185).

Disclosures. The authors declare that there are no conflicts of interest related to this article.

Data availability. Data underlying the results presented in this paper are not publicly available at this time but may be obtained from the authors upon reasonable request.

References

1. R. Horodecki, P. Horodecki, M. Horodecki, and K. Horodecki, "Quantum Entanglement," *Rev. Mod. Phys.* **81**(2), 865–942 (2009).

2. E. Schrödinger, "Discussion of Probability Relations between Separated Systems," *Math. Proc. Cambridge Philos. Soc.* **31**(4), 555–563 (1935).
3. E. Schrödinger, "Probability relations between separated systems," *Math. Proc. Cambridge Philos. Soc.* **32**(3), 446–452 (1936).
4. M. M. Cunha, A. Fonseca, and E. O. Silva, "Tripartite Entanglement: Foundations and Applications," *Universe* **5**(10), 209 (2019).
5. S. Xie and J. H. Eberly, "Triangle Measure of Tripartite Entanglement," *Phys. Rev. Lett.* **127**(4), 040403 (2021).
6. R.-H. Zheng, Y. Xiao, S.-L. Su, Y.-H. Chen, Z.-C. Shi, J. Song, Y. Xia, and S.-B. Zheng, "Fast and dephasing-tolerant preparation of steady Knill-Laflamme-Milburn states via dissipative Rydberg pumping," *Phys. Rev. A* **103**(5), 052402 (2021).
7. S. Liu, Y.-H. Chen, Y. Wang, Y.-H. Kang, Z.-C. Shi, J. Song, and Y. Xia, "Generation of cat states by a weak parametric drive and a transitionless tracking algorithm," *Phys. Rev. A* **106**(4), 042430 (2022).
8. S. Ghose, N. Sinclair, S. Debnath, P. Rungta, and R. Stock, "Tripartite Entanglement versus Tripartite Nonlocality in Three-qubit Greenberger-horne-zeilinger-class States," *Phys. Rev. Lett.* **102**(25), 250404 (2009).
9. Y. S. Weinstein, "Tripartite entanglement witnesses and entanglement sudden death," *Phys. Rev. A* **79**(1), 012318 (2009).
10. R. Uola, A. C. S. Costa, H. C. Nguyen, and O. Gühne, "Quantum steering," *Rev. Mod. Phys.* **92**(1), 015001 (2020).
11. I. Kogias, A. R. Lee, S. Ragy, and G. Adesso, "Quantification of Gaussian Quantum Steering," *Phys. Rev. Lett.* **114**(6), 060403 (2015).
12. J.-A. Larsson, "Loopholes in Bell inequality tests of local realism," *J. Phys. A: Math. Theor.* **47**(42), 424003 (2014).
13. J.-D. Bancal, C. Branciard, N. Brunner, N. Gisin, S. Popescu, and C. Simon, "Testing a Bell inequality in multipair scenarios," *Phys. Rev. A* **78**(6), 062110 (2008).
14. T. Beth and G. Leuchs, *Quantum information processing* (Wiley Online Library, 2005).
15. A. M. Childs, J. Preskill, and J. Renes, "Quantum information and precision measurement," *J. Mod. Opt.* **47**(2-3), 155–176 (2000).
16. Y. Xiang, X. Su, L. Mišta, G. Adesso, and Q. He, "Multipartite Einstein-Podolsky-Rosen steering sharing with separable states," *Phys. Rev. A* **99**(1), 010104 (2019).
17. Y. Xiang, I. Kogias, G. Adesso, and Q. He, "Multipartite Gaussian steering: Monogamy constraints and quantum cryptography applications," *Phys. Rev. A* **95**(1), 010101 (2017).
18. D. Bouwmeester, J.-W. Pan, K. Mattle, M. Eibl, H. Weinfurter, and A. Zeilinger, "Experimental quantum teleportation," *Nature* **390**(6660), 575–579 (1997).
19. S. Pirandola, J. Eisert, C. Weedbrook, A. Furusawa, and S. L. Braunstein, "Advances in quantum teleportation," *Nat. Photonics* **9**(10), 641–652 (2015).
20. Q. Y. He and M. D. Reid, "Einstein-Podolsky-Rosen paradox and quantum steering in pulsed optomechanics," *Phys. Rev. A* **88**(5), 052121 (2013).
21. S. Kiesewetter, Q. Y. He, P. D. Drummond, and M. D. Reid, "Scalable quantum simulation of pulsed entanglement and Einstein-Podolsky-Rosen steering in optomechanics," *Phys. Rev. A* **90**(4), 043805 (2014).
22. H. Tan, X. Zhang, and G. Li, "Steady-state one-way Einstein-Podolsky-Rosen steering in optomechanical interfaces," *Phys. Rev. A* **91**(3), 032121 (2015).
23. R. Schnabel, "Einstein-Podolsky-Rosen-entangled motion of two massive objects," *Phys. Rev. A* **92**(1), 012126 (2015).
24. H. Tan, W. Deng, Q. Wu, and G. Li, "Steady-state light-mechanical quantum steerable correlations in cavity optomechanics," *Phys. Rev. A* **95**(5), 053842 (2017).
25. Q. He and Z. Ficek, "Einstein-Podolsky-Rosen paradox and quantum steering in a three-mode optomechanical system," *Phys. Rev. A* **89**(2), 022332 (2014).
26. H. Tan and L. Sun, "Hybrid Einstein-Podolsky-Rosen steering in an atom-optomechanical system," *Phys. Rev. A* **92**(6), 063812 (2015).
27. Z.-B. Yang, X.-D. Liu, X.-Y. Yin, Y. Ming, H.-Y. Liu, and R.-C. Yang, "Controlling Stationary One-Way Quantum Steering in Cavity Magnonics," *Phys. Rev. Appl.* **15**(2), 024042 (2021).
28. C. Braggio, G. Carugno, M. Guarise, A. Ortolan, and G. Ruoso, "Optical Manipulation of a Magnon-Photon Hybrid System," *Phys. Rev. Lett.* **118**(10), 107205 (2017).
29. A. Kani, B. Sarma, and J. Twamley, "Intensive Cavity-Magnomechanical Cooling of a Levitated Macromagnet," *Phys. Rev. Lett.* **128**(1), 013602 (2022).
30. R.-C. Shen, J. Li, Z.-Y. Fan, Y.-P. Wang, and J. Q. You, "Mechanical Bistability in Kerr-modified Cavity Magnomechanics," *Phys. Rev. Lett.* **129**(12), 123601 (2022).
31. A. Sohail, R. Ahmed, J.-X. Peng, T. Munir, A. Shahzad, S. K. Singh, and M. C. de Oliveira, "Controllable Fano-type optical response and four-wave mixing via magnetoelastic coupling in an opto-magnomechanical system," *J. Appl. Phys.* **133**(15), 154401 (2023).
32. A. Sohail, R. Ahmed, J.-X. Peng, A. Shahzad, and S. K. Singh, "Enhanced entanglement via magnon squeezing in a two-cavity magnomechanical system," *J. Opt. Soc. Am. B* **40**(5), 1359–1366 (2023).
33. M. Amazioug, B. Teklu, and M. Asjad, "Enhancement of magnon-photon-phonon entanglement in a cavity magnomechanics with coherent feedback loop," *Sci. Rep.* **13**(1), 3833 (2023).

34. A. A. Houck, D. I. Schuster, J. M. Gambetta, J. A. Schreier, B. R. Johnson, J. M. Chow, L. Frunzio, J. Majer, M. H. Devoret, S. M. Girvin, and R. J. Schoelkopf, "Generating single microwave photons in a circuit," *Nature* **449**(7160), 328–331 (2007).
35. J. T. Hou and L. Liu, "Strong Coupling between Microwave Photons and Nanomagnet Magnons," *Phys. Rev. Lett.* **123**(10), 107702 (2019).
36. X. Zhang, C.-L. Zou, L. Jiang, and H. X. Tang, "Strongly Coupled Magnons and Cavity Microwave Photons," *Phys. Rev. Lett.* **113**(15), 156401 (2014).
37. C.-H. Bai, D.-Y. Wang, S. Zhang, S. Liu, and H.-F. Wang, "Strong mechanical squeezing in a standard optomechanical system by pump modulation," *Phys. Rev. A* **101**(5), 053836 (2020).
38. C. Kittel, "On the Theory of Ferromagnetic Resonance Absorption," *Phys. Rev.* **73**(2), 155–161 (1948).
39. H. Huebl, C. W. Zollitsch, J. Lotze, F. Hocke, M. Greifenstein, A. Marx, R. Gross, and S. T. B. Goennenwein, "High Cooperativity in Coupled Microwave Resonator Ferrimagnetic Insulator Hybrids," *Phys. Rev. Lett.* **111**(12), 127003 (2013).
40. Y. Tabuchi, S. Ishino, T. Ishikawa, R. Yamazaki, K. Usami, and Y. Nakamura, "Hybridizing Ferromagnetic Magnons and Microwave Photons in the Quantum Limit," *Phys. Rev. Lett.* **113**(8), 083603 (2014).
41. M. Goryachev, W. G. Farr, D. L. Creedon, Y. Fan, M. Kostylev, and M. E. Tobar, "High-Cooperativity Cavity QED with Magnons at Microwave Frequencies," *Phys. Rev. Appl.* **2**(5), 054002 (2014).
42. D. Zhang, X.-Q. Luo, Y.-P. Wang, T.-F. Li, and J. Q. You, "Observation of the exceptional point in cavity magnon-polaritons," *Nat. Commun.* **8**(1), 1368 (2017).
43. X. Zhang, C.-L. Zou, L. Jiang, and H. X. Tang, "Cavity magnomechanics," *Sci. Adv.* **2**(3), 1 (2016).
44. D. Lachance-Quirion, Y. Tabuchi, A. Gloppe, K. Usami, and Y. Nakamura, "Hybrid quantum systems based on magnonics," *Appl. Phys. Express* **12**(7), 070101 (2019).
45. G.-Q. Zhang, Z. Chen, D. Xu, N. Shammah, M. Liao, T.-F. Li, L. Tong, S.-Y. Zhu, F. Nori, and J. Q. You, "Exceptional Point and Cross-Relaxation Effect in a Hybrid Quantum System," *PRX Quantum* **2**(2), 020307 (2021).
46. L. Zhong, E. P. Menzel, R. D. Candia, P. Eder, M. Ihmig, A. Baust, M. Haeberlein, E. Hoffmann, K. Inomata, T. Yamamoto, Y. Nakamura, E. Solano, F. Deppe, A. Marx, and R. Gross, "Squeezing with a flux-driven Josephson Parametric Amplifier," *New J. Phys.* **15**(12), 125013 (2013).
47. A. Zorin, "Flux-Driven Josephson Traveling-Wave Parametric Amplifier," *Phys. Rev. Appl.* **12**(4), 044051 (2019).
48. J. Li, S.-Y. Zhu, and G. S. Agarwal, "Magnon-Photon-Phonon Entanglement in Cavity Magnomechanics," *Phys. Rev. Lett.* **121**(20), 203601 (2018).
49. J. Li, S.-Y. Zhu, and G. S. Agarwal, "Squeezed states of magnons and phonons in cavity magnomechanics," *Phys. Rev. A* **99**(2), 021801 (2019).
50. I. C. Skogvoll, J. Lidal, J. Danon, and A. Kamra, "Tunable Anisotropic Quantum Rabi Model via a Magnon–Spin-Qubit Ensemble," *Phys. Rev. Appl.* **16**(6), 064008 (2021).
51. B. Yurke, L. R. Corruccini, P. G. Kaminsky, L. W. Rupp, A. D. Smith, A. H. Silver, R. W. Simon, and E. A. Whittaker, "Observation of parametric amplification and deamplification in a Josephson Parametric Amplifier," *Phys. Rev. A* **39**(5), 2519–2533 (1989).
52. B. Yurke, P. G. Kaminsky, R. E. Miller, E. A. Whittaker, A. D. Smith, A. H. Silver, and R. W. Simon, "Observation of 4.2-k equilibrium-noise squeezing via a Josephson-Parametric Amplifier," *Phys. Rev. Lett.* **60**(9), 764–767 (1988).
53. R. Movshovich, B. Yurke, P. G. Kaminsky, A. D. Smith, A. H. Silver, R. W. Simon, and M. V. Schneider, "Observation of zero-point noise squeezing via a Josephson-parametric amplifier," *Phys. Rev. Lett.* **65**(12), 1419–1422 (1990).
54. M. A. Castellanos-Beltran, K. D. Irwin, G. C. Hilton, L. R. Vale, and K. W. Lehnert, "Amplification and squeezing of quantum noise with a tunable Josephson metamaterial," *Nat. Phys.* **4**(12), 929–931 (2008).
55. F. Mallet, M. A. Castellanos-Beltran, H. S. Ku, S. Glancy, E. Knill, K. D. Irwin, G. C. Hilton, L. R. Vale, and K. W. Lehnert, "Quantum State Tomography of an Itinerant Squeezed Microwave Field," *Phys. Rev. Lett.* **106**(22), 220502 (2011).
56. E. P. Menzel, R. Di Candia, F. Deppe, P. Eder, L. Zhong, M. Ihmig, M. Haeberlein, A. Baust, E. Hoffmann, D. Ballester, K. Inomata, T. Yamamoto, Y. Nakamura, E. Solano, A. Marx, and R. Gross, "Path Entanglement of Continuous-Variable Quantum Microwaves," *Phys. Rev. Lett.* **109**(25), 250502 (2012).
57. K. G. Fedorov, L. Zhong, S. Pogorzalek, P. Eder, M. Fischer, J. Goetz, E. Xie, F. Wulschner, K. Inomata, T. Yamamoto, Y. Nakamura, R. Di Candia, U. Las Heras, M. Sanz, E. Solano, E. P. Menzel, F. Deppe, A. Marx, and R. Gross, "Displacement of Propagating Squeezed Microwave States," *Phys. Rev. Lett.* **117**(2), 020502 (2016).
58. S. Kono, Y. Masuyama, T. Ishikawa, Y. Tabuchi, R. Yamazaki, K. Usami, K. Koshino, and Y. Nakamura, "Nonclassical Photon Number Distribution in a Superconducting Cavity under a Squeezed Drive," *Phys. Rev. Lett.* **119**(2), 023602 (2017).
59. A. Bienfait, P. Campagne-Ibarcq, A. H. Ktellerich, X. Zhou, S. Probst, J. J. Pla, T. Schenkel, D. Vion, D. Esteve, J. J. L. Morton, K. Moelmer, and P. Bertet, "Magnetic Resonance with Squeezed Microwaves," *Phys. Rev. X* **7**(4), 041011 (2017).
60. M. Malnou, D. A. Palken, L. R. Vale, G. C. Hilton, and K. W. Lehnert, "Optimal Operation of a Josephson Parametric Amplifier for Vacuum Squeezing," *Phys. Rev. Appl.* **9**(4), 044023 (2018).
61. C. W. Gardiner, "Inhibition of Atomic Phase Decays by Squeezed Light: A Direct Effect of Squeezing," *Phys. Rev. Lett.* **56**(18), 1917–1920 (1986).

62. D. Vitali, S. Gigan, A. Ferreira, H. R. Böhm, P. Tombesi, A. Guerreiro, V. Vedral, A. Zeilinger, and M. Aspelmeyer, "Optomechanical Entanglement between a Movable Mirror and a Cavity Field," *Phys. Rev. Lett.* **98**(3), 030405 (2007).
63. G. Vidal and R. F. Werner, "Computable measure of entanglement," *Phys. Rev. A* **65**(3), 032314 (2002).
64. G. Adesso, A. Serafini, and F. Illuminati, "Extremal entanglement and mixedness in continuous variable systems," *Phys. Rev. A* **70**(2), 022318 (2004).
65. M. B. Plenio, "Logarithmic Negativity: A Full Entanglement Monotone That is not Convex," *Phys. Rev. Lett.* **95**(9), 090503 (2005).
66. G. Adesso and F. Illuminati, "Entanglement in continuous-variable systems: recent advances and current perspectives," *J. Phys. A: Math. Theor.* **40**(28), 7821–7880 (2007).
67. G. Adesso and F. Illuminati, "Continuous variable tangle, monogamy inequality, and entanglement sharing in Gaussian states of continuous variable systems," *New J. Phys.* **8**, 15 (2006).
68. V. Coffman, J. Kundu, and W. K. Wootters, "Distributed entanglement," *Phys. Rev. A* **61**(5), 052306 (2000).
69. C.-G. Liao, H. Xie, R.-X. Chen, M.-Y. Ye, and X.-M. Lin, "Controlling one-way quantum steering in a modulated optomechanical system," *Phys. Rev. A* **101**(3), 032120 (2020).
70. X.-Y. Yin, Z.-B. Yang, Y.-M. Huang, Q.-M. Wan, R.-C. Yang, and H.-Y. Liu, "Enhancement of steady quantum entanglement and directional controllability of quantum steering in cavity magnetic hybrid systems," *Ann. Phys.* **535**(2), 2200603 (2023).
71. S. Armstrong, M. Wang, R. Y. Teh, Q. Gong, Q. He, J. Janousek, H.-A. Bachor, M. D. Reid, and P. K. Lam, "Multipartite einstein–podolsky–rosen steering and genuine tripartite entanglement with optical networks," *Nat. Phys.* **11**(2), 167–172 (2015).